Non-Data-Aided I/Q Mismatch Estimation in Low-IF Receivers

Gye-Tae Gil*, Young-Ik Song†, Yong H. Lee*

*Dept. of EECS, Korea Advanced Institute of Science and Technology, Taejon, 305-701, Korea
†R & D Team, Samsung Thales Co., Ltd, Korea
Email: yohlee@ee.kaist.ac.kr

***Abstract*— A digital signal processing (DSP) technique is presented that can compensate for the I/Q mismatch in low-IF receivers. In particular, a non-data-aided (NDA) I/Q mismatch estimator is derived by exploiting the statistical independence between the desired and image signals. The mean square error (MSE) of the estimate is analyzed. Computer simulation results indicate that the proposed technique can outperform existing adaptive DSP techniques that are based on the use of blind signal separation algorithms. It is observed that the image rejection ratio (IRR) of the proposed technique decreases monotonically with the number of observed samples for estimation, while that of conventional methods exhibits some floor.**

I. Introduction

A low-IF architecture uses quadrature mixing to down-convert a radio frequency (RF) signal to an intermediate frequency (IF) band, which in theory provides infinite attenuation of the image band and removes the need for analog image rejection filtering [1],[2]. This type of architecture has an advantage over direct-conversion in terms of robustness against DC offset and flicker noise. Although a low-IF architecture is a promising approach to the goal of single-chip radio receivers, its performance can be severely degraded by insufficient image rejection due to the I/Q mismatch. One approach to overcome such a problem is compensation by DSP. Off-line techniques that measure the mismatching effect from test signals were proposed in [3]-[5], while more sophisticated adaptive DSP techniques that apply a blind signal separation algorithm to the mismatch compensation were introduced in [6], [7]. The adaptive techniques do not need any test signals and are thus preferable to the off-line techniques. This is particularly true when the mismatch parameter is time-varying.

This letter introduces an alternative DSP technique that can also measure the effect of the I/Q mismatch directly from the received signal, without generating test signals. Unlike the schemes in [6] and [7], which are basically adaptive filters, the proposed technique is based on the use of an NDA mismatch estimator, which is derived by exploiting the statistical independence between the desired and image signals[1]. It is shown that the proposed compensator, consisting of the mismatch estimator followed by an image suppressor, can outperform existing adaptive DSP techniques.

[1]A data-aided I/Q mismatch estimator, which is mainly useful for direct conversion receivers, is introduced in [8].

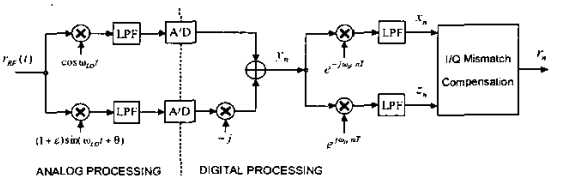

Fig. 1. Signal model.

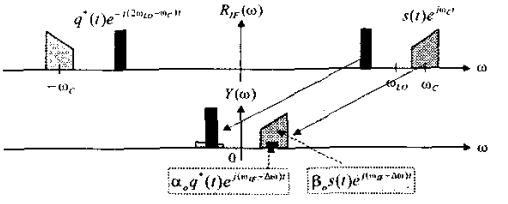

Fig. 2. Frequency domain interpretation of image band interference.

II. Signal Model

Fig. 1 shows the low-IF receiver. Assuming ideal filtering and no additive noise, the received RF signal $r_{RF}(t)$ is given by

$$r_{RF}(t) = 2\mathrm{Re}\{s(t)e^{j2\pi f_C t}\} + 2\mathrm{Re}\{q(t)e^{j2\pi f_I t}\} \quad (1)$$

where f_C is the carrier frequency, $f_I = f_C - 2(f_C - f_{LO})$ is the center frequency of the image band, f_{LO} is the local oscillator frequency, and $s(t)$ and $q(t)$ are the baseband equivalent expressions of the signals in the desired and image bands, respectively[2]. A quadrature mixer is used to down-convert the RF signal to a low-IF band, which then suffers from an amplitude mismatch ϵ and phase mismatch θ. These mismatches cause an image band signal to interfere with the desired signal as shown in Fig. 2. In addition, there is a frequency offset given by $\Delta f = f_{IF} - (f_C - f_{LO})$, where f_{IF} denotes the desired IF frequency. The digital signal $\{y_n\}$

[2]The signal model in (1) is reasonably valid even in a noisy environment, because $s(t)$ and $q(t)$ can represent "signal plus noise" in their respective bands.

after sampling at the rate $1/T$ can be expressed as

$$y_n = (\beta_o s_n + \alpha_o q_n^*)\, e^{j2\pi(f_{IF}+\Delta f)nT} + (\beta_o q_n + \alpha_o s_n^*)\, e^{-j2\pi(f_{IF}+\Delta f)nT}, \quad n = 0, 1, \ldots, N-1 \tag{2}$$

where $\beta_o = \frac{1}{2}[1 + (1+\epsilon)e^{-j\theta}]$, $\alpha_o = \frac{1}{2}[1 - (1+\epsilon)e^{j\theta}]$, $s_n = s(t)|_{t=nT}$, $q_n = q(t)|_{t=nT}$. The two baseband signals, $\{x_n\}$ and $\{z_n\}$, obtained by down-converting y_n in the digital domain, are given by

$$x_n = \beta_o s_n e^{j2\pi n\nu} + \alpha_o \left(q_n e^{-j2\pi n\nu}\right)^* \tag{3}$$

and

$$z_n = \beta_o q_n e^{-j2\pi n\nu} + \alpha_o \left(s_n e^{j2\pi n\nu}\right)^* \tag{4}$$

where ν is the normalized carrier-frequency offset given by $\nu = \Delta f T$. When $\nu = 0$, the signal model in (3) and (4) becomes identical to the one in [7] and a special case of the model in [6], which considers a broadband I/Q mismatch.

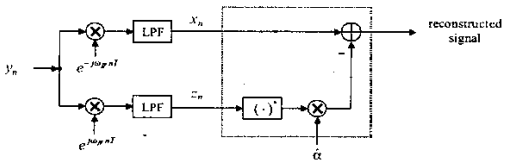

Fig. 3. I/Q mismatch compensation structure.

III. Proposed Technique

If α_o and β_o in (3) and (4) are known, then the image signal can be suppressed by exploiting the following relation:

$$x_n - \alpha z_n^* = \left(1 - |\alpha|^2\right) \beta_o s_n e^{j2\pi n\nu} \tag{5}$$

where $\alpha = \alpha_o/\beta_o^*$. The parameter α will be referred to as the *I/Q mismatch* parameter. It is straightforward to show that $|\alpha| < 1$ if $|\theta| < \pi/2$. The right-hand-side (RHS) of (5) represents the reconstructed signal in the desired band, which is a scaled version of $s_n e^{j2\pi n\nu}$ and can be obtained by the mismatch compensation structure in Fig. 3 when $\hat{\alpha} = \alpha$. A dual equation of (5) can be written as

$$z_n - \alpha x_n^* = \left(1 - |\alpha|^2\right) \beta_o q_n e^{-j2\pi n\nu}. \tag{6}$$

It is assumed that the desired signal $\{s_n\}$ and image signal $\{q_n^*\}$ are zero-mean wide-sense stationary (WSS) processes that are statistically independent to each other and asymptotically uncorrelated ($\lim_{k\to\infty} E[s_n s_{n-k}^*] = 0$, $\lim_{k\to\infty} E[q_n^* q_{n-k}] = 0$). From (5) and (6) it is possible to show that

$$E\left[(x_n - \alpha z_n^*)^* (z_n - \alpha x_n^*)^*\right] = (1 - |\alpha|^2)^2 (\beta_o^*)^2 E[s_n^* q_n^*] = 0. \tag{7}$$

Under the assumptions stated above, $\{s_n^* q_n^*\}$ is an asymptotically uncorrelated WSS process and mean-ergodic [9]. Therefore, (7) can be approximated as

$$\frac{1}{N}\sum_{n=0}^{N-1} \left[(x_n - \alpha z_n^*)^* (z_n - \alpha x_n^*)^*\right] \cong 0 \tag{8}$$

for a large N. Solving (8) for α results in $\hat{\alpha}$, which is an estimate of α:

$$\hat{\alpha} = \frac{b \pm \sqrt{b^2 - 4|c|^2}}{2c^*} \tag{9}$$

where $b = \sum_{n=0}^{N-1} \left(|x_n|^2 + |z_n|^2\right)$ and $c = \sum_{n=0}^{N-1} x_n z_n$. Using the Cauchy-Schwartz inequality, it is straightforward to show that $b^2 - 4|c|^2 \geq 0$. Let $\mathbf{x} = [x_0; x_1, \cdots, x_{N-1}]^T$ and $\mathbf{z} = [z_0, z_1, \cdots, z_{N-1}]^T$. Then,

$$\begin{aligned} b^2 - 4|c|^2 &= \left(\|\mathbf{x}\|^2 + \|\mathbf{z}\|^2\right)^2 - 4|<\mathbf{x}, \mathbf{z}>|^2 \\ &\geq \left(\|\mathbf{x}\|^2 + \|\mathbf{z}\|^2\right)^2 - 4\|\mathbf{x}\|^2\|\mathbf{z}\|^2 \\ &= \left(\|\mathbf{x}\|^2 - \|\mathbf{z}\|^2\right)^2 \geq 0 \end{aligned} \tag{10}$$

where the first inequality comes from Cauchy-Schwartz inequality of $|<\mathbf{x}, \mathbf{z}>|^2 \leq \|\mathbf{x}\|^2\|\mathbf{z}\|^2$. In (9), let $\alpha_1 = \frac{b - \sqrt{b^2-4|c|^2}}{2c^*}$ and $\alpha_2 = \frac{b + \sqrt{b^2-4|c|^2}}{2c^*}$. Then, $\alpha_2 = 1/\alpha_1^*$ and $|\alpha_1| \leq |\alpha_2|$. These facts indicate that $|\alpha_1| \leq 1$ and $|\alpha_2| \geq 1$. Thus α is estimated by α_1 ($\hat{\alpha} = \alpha_1$) and α_2 discarded, because $|\alpha| < 1$ whenever $|\theta| < \pi/2$.

IV. Performance Analysis

As shown in the Appendix, the estimate $\hat{\alpha}$ is approximately unbiased ($E[\hat{\alpha}] \cong \alpha$) and its MSE can be approximated as

$$E[|\alpha - \hat{\alpha}|^2] \cong \frac{1}{\kappa_q/\rho + \kappa_s\rho - 2 + (N-1)\left(1/\rho + \rho + 2\right)} \tag{11}$$

when $\{s_n\}$ and $\{q_n\}$ are independent identically distributed (i.i.d) complex random variables with a zero mean. In (11), κ_s and κ_q denote the kurtosis of s_n and q_n, respectively, given by $\kappa_s = E[|s_n|^4]/E[|s_n|^2]^2$ and $\kappa_q = E[|q_n|^4]/E[|q_n|^2]^2$, where ρ is the input signal-to-image ratio (SIR) defined as $\rho = E[|s_n|^2]/E[|q_n^*|^2]$. It is interesting to note that the MSEs corresponding to ρ and $1/\rho$ are identical when $\kappa_s = \kappa_q$. This occurs because of the duality between x_n in (3) and z_n in (4). Given κ_s, κ_q, and N, the MSE is upper bounded by $1/(4N + \kappa_q + \kappa_s - 6)$, which is the MSE for $\rho = 1$ (input SIR = 0 [dB]) and decreases monotonically with N and ρ ($1/\rho$) when $\rho > 1$ ($\rho < 1$). It is also interesting to note that for large N the MSE is almost not sensitive to the values of κ_s and κ_q.

TABLE I
Computational Load with Single-Tap Adaptive Filters.

Algorithm	Real products	Real additions
proposed	$8N + 2$	$6N + 4$
method in [6]	$20N - 12$	$16N - 8$
method in [7]	$96N - 56$	$74N - 46$

The computational complexity are summarized in Table I. In writing the figures, it was assumed that the methods in [6] and [7] used single-tap adaptive filters to suppress the image interference. The proposed method needs a additional square-root operation when the mismatch estimate is evaluated. Nevertheless, the proposed method is less complex than the existing methods in [6] and [7].

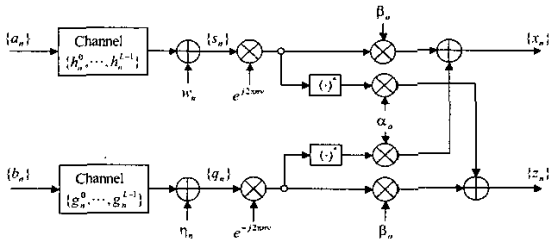

Fig. 4. System model used for simulation.

V. Simulation

Computer simulations were conducted to examine the performance of the proposed estimator. Fig. 2 shows the system model used for the simulation. The baseband equivalent signals in the desired and image bands are expressed by $s_n = \sum_{l=0}^{L-1} h_n^l a_{n-l} + w_n$ and $q_n = \sum_{l=0}^{L-1} g_n^l b_{n-l} + \eta_n$, respectively, where $\{a_n\}$ and $\{b_n\}$ are the transmitted symbols that are quadrature phase-shift keying (QPSK), $\{h_n^l | l = 0, 1, \cdots, L-1\}$ and $\{g_n^l | l = 0, 1, \cdots, L-1\}$ denote the channel responses at time n, and $\{w_n\}$ and $\{\eta_n\}$ denote additive white Gaussian noise (AWGN). The signal-to-noise ratios (SNRs) of the received signals $\{s_n\}$ and $\{q_n\}$ were 20 [dB]. Two types of channels were considered: AWGN channels ($L = 1$, $h_n^0 = g_n^0 = 1$) and Rayleigh fading channels with eight paths ($L = 8$) that had an identical average power and $f_D T = 0.01$, where f_D is the maximum Doppler frequency. The frequency offset $\nu = 0.01$. The amplitude mismatch $\epsilon = 0.1$ and phase mismatch $\theta = 10°$ ($\alpha_o = -0.0416 - j0.0955$, $\beta_o = 1.0416 - j0.0955$, and $\alpha = -0.048 - j0.0873$). The input SIR $\rho \in \{0, \pm 10, \pm 20, \pm 30\}$ [dB]. In the simulation, the MSE and image rejection ratio (IRR)[10], which is the ratio between the input SIR ρ and the SIR of $x_n - \hat{\alpha} z_n^*$, were empirically estimated based on 100 trials. Since the image suppressed signal is represented by $x_n - \hat{\alpha} z_n^* = (1 - \hat{\alpha}\alpha^*)\beta_o s_n e^{j2\pi n\nu} + (\alpha - \hat{\alpha})(\beta_o q_n e^{-j2\pi n\nu})^*$, the SIR of $x_n - \hat{\alpha} z_n^*$ is given by $\frac{|(1-\hat{\alpha}\alpha^*)\beta_o|^2 E[|s_n|^2]}{|(\alpha-\hat{\alpha})\beta_o^*|^2 E[|q_n^*|^2]}$, which indicates that the IRR is equal to $\frac{|\alpha-\hat{\alpha}|^2}{|1-\hat{\alpha}\alpha^*|^2}$.

Fig. 5 shows the MSEs obtained from the analysis and simulation for the AWGN channels. A remarkably good agreement was observed between the analytical and simulation results. As expected, the MSE decreased monotonically with N and ρ ($1/\rho$) when $\rho > 1$ ($\rho < 1$). When the image-band signal power was zero, the proposed estimator exhibited extremely small MSEs as shown in Fig. 6.

Figs. 7 and 8 show the IRRs for the AWGN and Rayleigh fading channels, respectively. For comparison, the figures also show the IRRs for the adaptive image canceller in [6], whose filtering and weight update equations are represented as follows: $\hat{s}_n = x_n - w_n^{(1)} z_n$ and $\hat{q}_n = z_n - w_n^{(2)} x_n$, where the weights are updated by $w_{n+1}^{(1)} = w_n^{(1)} + \mu \hat{q}_n \hat{s}_n^*$ and $w_{n+1}^{(2)} = w_n^{(2)} + \mu \hat{s}_n \hat{q}_n^*$. The stepsize μ was set at 0.0001. Comparing the IRR curves in Figs. 7 and 8 indicates that

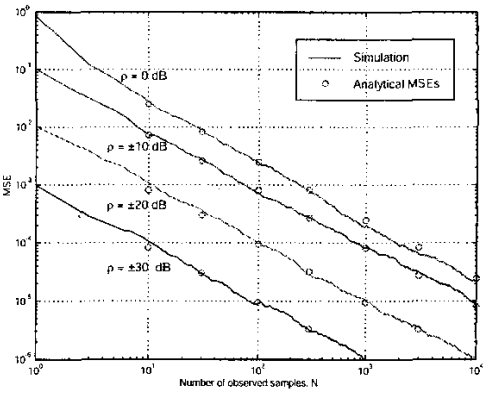

Fig. 5. MSE performance of proposed estimator for AWGN channels.

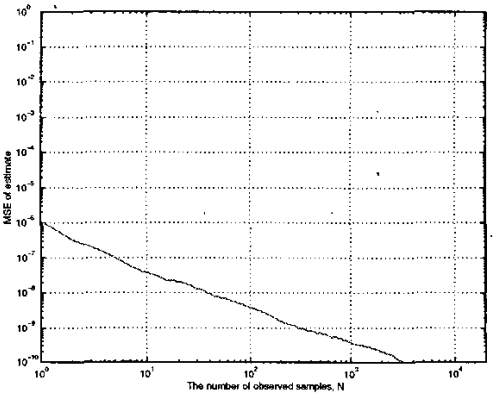

Fig. 6. MSE performances of proposed estimator for AWGN channels when the image-band signal power was zero.

neither technique was vulnerable to the channel type: the IRR curves for the AWGN channels were almost identical to the corresponding IRR curves for the Rayleigh fading channels. The proposed method outperformed the adaptive canceller in [6] when the number of observed samples N was greater than or equal to 11. Furthermore, the IRR of the former decreased monotonically with N, while the IRR curves of the latter exhibited some floor.

The number of samples required to achieve a specific value of the output SIR can be of interest. In Fig. 7 and 8, it is estimated that the IRR is approximately equal to ρ/N when $\rho \ll 1$, meaning that the proposed method needs at least $10^{0.1\eta}$ samples to achieve the output SIR of η dB.

VI. Conclusion

An NDA I/Q mismatch estimator for low-IF receivers was developed and applied to I/Q mismatch compensation. It was shown that the MSE of the estimator and IRR of the resulting compensator decreased monotonically with the number of observed samples, while the IRR curves of an

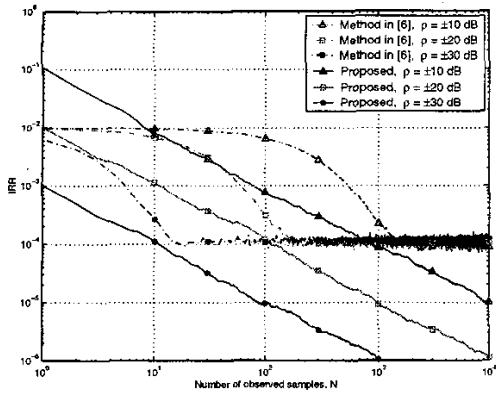

Fig. 7. IRR performances for AWGN channels.

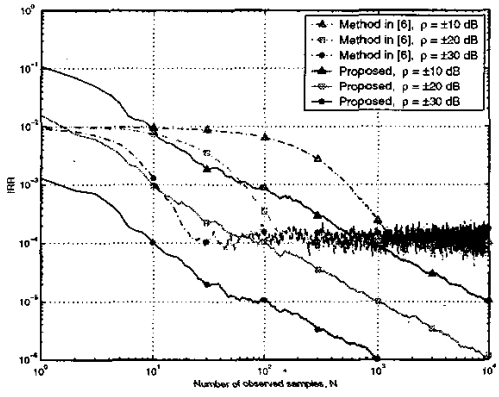

Fig. 8. IRR performances for frequency-selective fading channels.

existing adaptive technique exhibited some floor. In contrast to the adaptive techniques in [6] and [7], both of which require some caution to guarantee convergence of the algorithm, the proposed compensator is free from convergence issues.

APPENDIX

Denote the left-hand-side (LHS) of (8) by γ. Then

$$\begin{aligned}\gamma &= \frac{1}{N}\sum_{n=0}^{N-1}\left[(x_n-\alpha z_n^*)^*(z_n-\alpha x_n^*)^*\right] \\ &= \frac{(1-|\alpha|^2)^2(\beta_o^*)^2}{N}\sum_{n=0}^{N-1}s_n^*q_n^*\end{aligned} \tag{A1}$$

and α can be expressed as

$$\alpha = \frac{1}{2c^*}(b-\sqrt{b^2-4|c|^2+4c^*N\gamma}). \tag{A2}$$

Approximating $\sqrt{b^2-4|c|^2+4c^*N\gamma}$ by $\sqrt{b^2-4|c|^2}+\frac{4c^*N\gamma}{2\sqrt{b^2-4|c|^2}}$, which is a first-order Taylor series expansion of $\sqrt{b^2-4|c|^2+4c^*N\gamma}$ in the vicinity of $\gamma=0$, results in $\alpha \cong \hat{\alpha}-\frac{\gamma}{\sqrt{u}}$, where $\hat{\alpha}=\alpha_1$ in (9) and $u=\frac{b^2-4|c|^2}{N^2}$. Then, for large N, $E[\hat{\alpha}]\cong\alpha$ and

$$E[|\alpha-\hat{\alpha}|^2] \cong \frac{E\left[|\gamma|^2\right]}{E\left[u\right]}. \tag{A3}$$

Assuming that $\{s_n\}$ and $\{q_n\}$ are i.i.d complex random variables with a zero mean, it can be shown that

$$E\left[|\gamma|^2\right] = \frac{(|\beta_o|^2-|\alpha_o|^2)^2}{N}\sigma_s^2\sigma_q^2 \tag{A4}$$

and

$$\begin{aligned}E\left[u\right] = &\frac{(|\beta_o|^2-|\alpha_o|^2)^2}{N}\left(\kappa_s\sigma_s^4+\kappa_q\sigma_q^4-2\sigma_s^2\sigma_q^2\right) \\ &+\frac{(|\beta_o|^2-|\alpha_o|^2)^2(N-1)}{N}\left(\sigma_s^2+\sigma_q^2\right)^2\end{aligned} \tag{A5}$$

where $\sigma_s^2=E[|s_n|^2]$, $\sigma_q^2=E[|q_n|^2]$, $\kappa_s=E\left[|s_n|^4\right]/\sigma_s^4$ and $\kappa_q=E\left[|q_n|^4\right]/\sigma_q^4$. Using these results in (A3), the RHS of (11) can be obtained.

REFERENCES

[1] J. Crols and M. S. J. Steyaert, "Low-IF topologies for high-performance analog front ends of fully integrated receivers," *IEEE Trans. Circuits and Systems*, vol. 45, no. 3, pp. 269–282, Mar. 1998.

[2] S. Mirabbasi and K. Martin, "Classical and modern receiver architectures," *IEEE Commun. Mag.*, vol. 38, no. 11, pp. 132–139, Nov. 2000.

[3] F. E. Churchill, G. W. Ogar and B. J. Thomson, "The correction of I and Q errors in a coherent processor," *IEEE Trans. Aerosp. Electronic Systems*, vol. AES-17, no. 1, pp. 131–137, Jan. 1981.

[4] R. A. Green, R. Anderson-sprecher, and J. W. Pierre, "Quadrature receiver mismatch calibration," *IEEE Trans. Signal Processing*, vol. 47, no. 11, pp. 3130–3133, Nov. 1999.

[5] C. C. Chen and C. C. Huang, "On the architecture and performance of a hybrid image rejection receiver," *IEEE J. Select. Areas Commun.*, vol. 19, pp. 1029-1040, Jun. 2001.

[6] L. Yu and W. M. Sneglove, "A novel adaptive mismatch cancellation system for quadrature IF radio receivers," *IEEE Trans. Circuits and Systems II*, vol. 46, no. 6, pp. 789–801, June 1999.

[7] M. Valkama, M. Renfors, and V. Koivunen, "Advanced methods for I/Q imbalance compensation in communication receivers," *IEEE Trans. Signal Processing*, vol. 49, pp. 2335–2344, Oct. 2001.

[8] I. H. Sohn, E. R. Jeong, and Y. H. Lee, "Data-aided approach to I/Q mismatch and DC offset compensation in communication receivers," *IEEE Commun. Letter*, vol. 6, no. 12, pp. 547–549, Dec. 2002.

[9] M. H. Hayes, *Statistical digital signal processing and modeling*, John Wiley & Sons, Inc., 1996.

[10] B. Razavi, *RF microelectronics*, Prentice Hall, 1998.